Electrochemical CO2 reduction on gas diffusion electrodes: enhanced selectivity of In–Bi bimetallic particles and catalyst layer optimization through a design of experiment approach

Philips, M.F.; Pavesi, D,; Wissink, T.; Costa Figueiredo, M.C.; Gruter, G.J.M.; Koper, M.T.M.; Schouten, K.J.P.

ACS APPLIED ENERGY MATERIALS

www.acsaem.org Article

Electrochemical CO_2 Reduction on Gas Diffusion Electrodes: Enhanced Selectivity of In−Bi Bimetallic Particles and Catalyst Layer Optimization through a Design of Experiment Approach

Matthew F. Philips,[#] Davide Pavesi,[#] Tim Wissink, Marta C. Figueiredo, Gert-Jan M. Gruter, Marc T. M. Koper, and Klaas Jan P. Schouten*

Cite This: *ACS Appl. Energy Mater.* 2022, 5, 1720−1730 Read Online

ACCESS | Metrics & More | Article Recommendations | Supporting Information

ABSTRACT: CO_2 electroreduction to formate powered by renewable energy is an attractive strategy to recycle carbon. Electrode materials showing high selectivity for formate at high current densities are post-transition metals such as Sn, In, Pb, Hg, and Bi. Scaling up the CO_2 electroreduction technology to industrial size will require, among other things, maximization of selectivity at high current densities. We show here that InBi electrocatalysts provide enhanced selectivity compared to pure In and Bi and that a proper formulation of the catalyst layer can have a profound impact on the performance of gas diffusion electrode electrolyzers. The best performing electrodes screened in this study show nearly 100% current efficiency at current densities up to 400 mA cm^{-2} for 2 h. Additionally, one electrode was shown to operate at a current density of 200 mA cm^{-2} for 48 h at a current efficiency of 85% and remained operating with a current efficiency above 50% for 124 h.

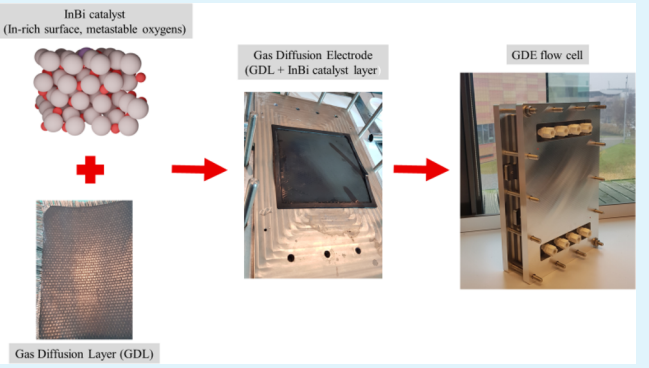

KEYWORDS: *electrochemistry, CO2 reduction, gas diffusion electrode, bimetallic particles, catalyst optimization, formate*

INTRODUCTION

The electrocatalytic conversion of CO_2 is of considerable interest nowadays due to the possibility of using energy from renewable sources to convert this ubiquitous and rather inert waste product to value-added chemicals and fuels.[1] The reaction can yield several products such as CO, methane, ethylene, and formic acid. Among these, formic acid is of particular interest because of its possible use as a liquid fuel precursor and hydrogen carrier for fuel cell applications[2] and because of its existence in the market as a preservative for animal feed and in the production of leather. The formic acid salt (formate) can be used as a precursor to C2 chemicals such as oxalic acid, glyoxylic acid, and glycolic acid, thus enabling further conversions.[3−5] The small number of electrons (two) needed for the conversion of CO_2 to formic acid and formate and the relatively high molecular weight of the product allow for higher production rates with a smaller number of electrochemical cells in a stack, lowering the capital and operational costs. On top of this, the reaction has a high atomic efficiency (100%), meaning that every atom present in the CO_2 reactant is preserved in the final product, thus avoiding the production of unnecessary waste and making this conversion one of the most economically promising electrocatalytic conversions.[6−9] However, high current densities, high current efficiencies, and long electrode lifetimes are required for the technology to be economically feasible.

Typically, catalysts based on metals such as Sn, In, Pb, Hg, and Bi are used for formate production as they attain a high current efficiency (CE).[10] High current densities are obtained by using gas diffusion electrode (GDE) configurations. GDEs can achieve high current efficiencies at high current densities because they overcome mass transport limitations arising from the low solubility of CO_2 in aqueous electrolytes.[11] However, GDEs are much more complex than a typical 3D metallic electrode, and there have been limited optimization and stability studies for this reaction.[12]

A GDE consists of a gas diffusion layer (GDL) and a catalyst layer. Both these layers can affect the performance of the GDE and should be considered for the total optimization of the electrode. The effect of the GDL has been hardly studied in this reaction, while the catalyst layer characteristics have

Received: October 8, 2021
Accepted: January 5, 2022
Published: January 19, 2022

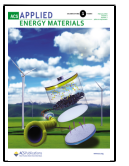

https://doi.org/10.1021/acsaem.1c03156
ACS Appl. Energy Mater. 2022, 5, 1720−1730

received the most attention. The type of binder used in the catalyst layer has been shown to give various performances of GDEs.[12] The catalyst loading has been shown to shift product distributions between formate and CO.[13] Yet, the amount of catalyst supported on carbon and the binder amount in the catalyst layer have also been scarcely studied for this reaction. Furthermore, most published results for this reaction have a run time of less than 8 h, and consequently, the stability of GDEs for this reaction has not been well assessed. The current state of the art in current density for this reaction appears to be the study by Löwe et al., where they achieve 1800 mA/cm^2 with 70% CE toward formate for 45 min.[14] Additionally, the longest operated GDE for this reaction that we have found was from the paper by Yi et al., where the performance of a Bi GDE was monitored for 564 h in a potentiostatic experiment, with the average current density <100 mA/cm^2.[15]

In this work, we provide a rationale for the enhanced performance of Avantium's patented InBi electrocatalyst, described in detail in the patent, by comparing it to pure In and Bi catalysts synthesized in the same way.[16] We then use this superior catalyst in the design of experiments (DOE) to optimize a GDE. The DOE investigates the effect of the GDL type, catalyst loading, amount of catalyst supported on carbon, binder amount, binder type, and current density on the CE toward formate, the cell potential, and the electrode stability. This is the first study of which we are aware that investigates the possible interactions between catalyst layer characteristics and different GDL structures for the electrochemical conversion of CO_2 toward formate. Additionally, all of the studies that we have encountered for this reaction attempt to optimize the performance using one-factor-at-a-time approach which can result in finding a local optimum rather than a global optimum. The DOE approach, instead, can help to find a global optimum by taking into account interactions between multiple factors.[17] The goal of this study is to identify several factors and interactions between the factors investigated that influence the CE toward formate and the cell potential. The significance of the interactions shows that several considerations should be made when comparing results between studies or designing future studies. A definitive explanation of the reasons behind the significance of factors is beyond the scope of this study and should be the object of future investigations.

EXPERIMENTAL METHODS

Materials and Chemicals. $InCl_3$ (99.999%) and trisodium citrate dihydrate (>99%) were purchased from Aldrich. Vulcan Carbon (VXC72R) was purchased from Cabot Corp. Carbon Cloth (60% Teflon-treated), and Nafion solution (5 wt % solution) was obtained from the Fuel Cell Store. $KHCO_3$ (99.5%), H_2SO_4 (95%) solution in water, and $NaBH_4$ (98+%) were purchased from Acros Organics. Triethylene glycol (TEG; 99%) and $Bi(NO_3)_3{\cdot}5H_2O$ (98%) were purchased from Alfa Aesar. PVDF Kynar flex 2801 was purchased from Arkema.

Particle Production and Ink Formulation. The carbon-supported particles were prepared in TEG via the chemical reduction method described in the patent.[16] For the synthesis of the bimetallic InBi catalysts (50:50 wt %), 1.64 g of $InCl_3$ and 1.98 g of $Bi(NO_3)_3{\cdot}5H_2O$ were dissolved in 250 mL of TEG along with 1.14 g of trisodium citrate dihydrate. The mixture was stirred and heated to 60 °C under a N_2 atmosphere until the salts were dissolved. Different amounts of Vulcan carbon were added according to the desired metal loading on carbon (30, 60, or 90 wt %), and the mixture was stirred overnight. An overview of the different amounts of carbon can be found in Table 1. The resulting suspension was heated to 100 °C, and the N_2 atmosphere was switched to an Ar atmosphere. When the desired temperature was reached, 4.5 mL of a 12.5 M $NaBH_4$ solution was added over 40 s. After this, the mixture was let to react for 15 min before being cooled down, filtered, and washed several times with isopropanol and isopropanol/water mixtures. For the single metals, a similar procedure was used: the reaction was scaled down to 100 mL, and 1.1 g of $InCl_3$ was used for the In-only catalyst, while 2.4 g of $Bi(NO_3)_3{\cdot}5H_2O$ was used for the Bi-only catalyst. The amount of carbon was chosen such that the atomic % of metal on carbon rather than the weight % on carbon of the single metal catalyst would be similar to the 60 wt % InBi on carbon (53.7 wt % In on C and 67.9 wt % Bi on carbon). The InBi catalysts with different loadings on carbon were used for the DOE, while the single metal catalysts were compared to InBi 60 wt % on carbon for benchmarking and characterization.

Table 1. Amounts of C Used for Synthesis

	composition	
catalyst	wt % on C	g Vulcan C
InBi/C	30	4.4
InBi/C	60	1.0
InBi/C	90	0.2
In/C	53.7	0.5
Bi/C	67.9	0.5

Two types of binders were investigated in this study: PVDF and Nafion. The inks were formulated according to the binder used. In the case of Nafion, the catalysts were sonicated in isopropanol before the addition of the binder, while for PVDF, a mixture of isopropanol and acetone was used as a solvent to avoid the precipitation of the binder. Three different binder loadings were tested: 10, 20, and 30 wt % of dry binder in the catalyst layer. The amounts of binder added to the ink were chosen according to the catalyst weight in the ink.

The inks were airbrushed on homemade GDLs, aiming to reach three different theoretical metal loadings: 0.5, 1.25, and 2 mg_{metal} cm^{-2}.

Gas Diffusion Layer Production. The synthesis method for the GDLs in this study was modified from a patented process.[18] 8.92 mL of PTFE DISP 30 was added to 70 mL of a 1:1 volume IPA/water mixture and stirred for 1 min before mixing with 15 g of Soltex Acetylene Black 75%-03 carbon in a Bourgini mixer. After 1 min of mixing, a dough-like mixture was collected. A rolling pin was used to prepare the dough for a cross-rolling technique to obtain the desired thickness, where the thickness setting is a discrete numerical factor. A rectangle of about 250 cm^2 was cut from this structure, and a paint roller was used to apply PTFE DISP 30 diluted to 50% with a 1:1 volume IPA/H_2O to the back of the dough. Fiber Glast 1K plain weave carbon fiber fabric was used as the current collector and placed on top of the PTFE-applied layer. A Carver heated press (model number 4533) was used to press the structure in three stages at various temperatures, pressures, and durations according to the two tested GDL methods shown in Table 2. GDLs of 4.4 cm × 4 cm were

Table 2. GDL Production Conditions

production process condition	GDL 1	GDL 2
PTFE wt %	35	35
rolling thickness setting	4	4
time stage 1 (min)	60	32.5
pressure stage 1 (ton)	20	10.25
temp stage 1 (°C)	200	140
time stage 2 (min)	60	32.5
pressure stage 2 (ton)	20	10.25
temp stage 2 (°C)	335	307.5
time stage 3 (min)	60	32.5
pressure stage 3 (ton)	25	13
temp stage 3 (°C)	335	317.5

https://doi.org/10.1021/acsaem.1c03156
ACS Appl. Energy Mater. 2022, 5, 1720−1730

cut from the final structures. A schematic of the GDLs synthesized from the above method, and a picture of our GDL 2 structure (GDL 1 and GDL 2 look virtually identical on a macroscopic scale) are shown in the Supporting Information (Figures S1 and S2).

Electrochemical Measurements. Cyclic voltammetry (CV) was carried out in a cell connected to a BioLogic MPG2 potentiostat (with EC-Lab Software version 11.10). A leak-free Ag/AgCl electrode was used as the reference electrode, and the counter electrode was a Pt gauze. The working electrode was a carbon cloth on which the catalytic ink was drop-casted. The electrolyte was a 0.5 M $KHCO_3$ solution, saturated with either CO_2 or N_2 before running the experiments. The electrodes, with an exposed area of 1 cm^2, were cycled at a scan rate of 50 mV/s, with N_2 or CO_2 continuously purging the headspace of the cell.

Particle Characterization. X-ray diffraction patterns of the particles supported on carbon were obtained by a Philips X'pert equipped with X-lerator in a 2θ range from 20 to 80°. SEM was performed on an Apreo SEM system equipped with an energy-dispersive X-ray analyzer. X-ray photoelectron spectroscopy (XPS) measurements were performed on the catalyst powders with a Thermo Fisher K-alpha instrument. Differential scanning calorimetry was performed on a Mettler Toledo DSC 3+ Stare system at a scan rate of 5 °C per minute between 25 and 300 °C two times. The composition of the particles and the actual loading on the carbon support were investigated by inductively coupled plasma spectroscopy (ICP).

Flow Cell Electrolysis. Electrolysis was carried out in a commercial 10 cm^2 GDE flow cell (ElectroCell, Micro Flow Cell). The anode and the cathode were separated by a reinforced Nafion membrane N324. The anolyte was a 0.5 M H_2SO_4 solution, and the anode catalyst was a Ti current collector coated with Ir/RuO_2. The anodic reaction was the oxygen evolution reaction. The catholyte was a 0.5 M $KHCO_3$ solution, and the cathode was a GDE airbrushed with one of the synthesized catalysts. The electrolyte solutions were circulated in a closed-loop in the compartments at a flow rate of 50 mL/min with a peristaltic pump. This was done to accumulate formate for analysis and to reduce the electrolyte utilization. CO_2 was fed through the GDE in the cathodic compartment at a flow rate of 50−100 mL/min, depending on the current. The cell was connected to a power supply and operated galvanostatically.

The samples of the catholyte were collected, neutralized with HCl, and analyzed for soluble products with a PerkinElmer Lambda 35 UV−vis spectrometer.

DOE for Catalyst Layer Optimization. The Custom Design platform in JMP was used to generate a DOE for this study to investigate the effect of the following parameters on the cell potential, CE toward formate, and electrode stability: GDL, loading of the metal catalyst, amount of catalyst supported on carbon, the weight percentage of binder in the catalyst layer, binder type, and current density.[19] The GDL and binder type were designated as categorical variables, while the others were continuous. All second order interactions and quadratic terms were considered for a model. This resulted in an experimental matrix of 32 runs shown in the results section. Each GDE was operated for 120 min using the same conditions as mentioned above at the current density specified by the DOE. After the first 120 min, each GDE was operated at the other two current densities for 120 min each. Thus, each GDE was operated for a total of 6 h at three current densities. Additionally, three runs were repeated to demonstrate the repeatability of the system. These data are shown in the Supporting Information Figures S3−S5.

Extended Operation Experiments. Two experiments were performed as extended operation runs to determine the lifetime stability of these electrodes. The two electrodes used for the experimental run 5 were used for these extended operation experiments. Therefore, each electrode for these experiments was operated for 6 h in the DOE set prior to running the extended experiments. Each electrode was operated at a different constant current density until the CE of formate decreased below 50%. Additionally, every 24 h, the current to the electrochemical cell was set to zero, the cathode compartment was rinsed with deionized water, and air was passed through the cathode compartment for 1 h to regenerate the electrode before restarting the cell at the operating current density.[20]

DOE Analysis Workflow. After all of the runs were performed and repeats demonstrated repeatability, the stepwise platform in JMP was used to generate models for the CE toward formate, the cell potential, and the electrode stability. All factors, two-way interactions, and square terms were considered for the model. Multiple linear regression was used to generate two models for each response, one using the Bayesian information criterion (BIC) and the other using the Akaike information criterion as a stopping rule to help prevent overfitting.[21,22] The models generated were in the form of eq 1

$$y = b_1X_1 + b_2X_2 + b_3X_3 + \ldots + b_nX_n \quad (1)$$

where b_n is the model term coefficient, and X_n is the factor variable which can be a multiplicative combination of two factors (for interactions) or a squared factor (to model curvature).

The model which used the BIC stopping rule was chosen for the CE toward formate, while both methods resulted in the same model for the cell potential. A comparison between the models generated from the two stopping rules and the reasoning for model selection can be found in the Supporting Information (Figures S7−S10). The model terms in the selected models were then sorted based on the coefficients of scaled model terms which can be used to show the terms which affect the response the greatest.[17] Model terms with p values less than 0.01 (99% confidence) are discussed in more detail for each model.

RESULTS

Flow Cell Electrolysis: Benchmarking InBi Against Single Metals. The performance of the InBi catalyst was benchmarked against In and Bi single-metal catalysts by comparing the CE of CO_2 electroreduction to formate at 200 mA cm^{-2} for 4 h. The catalyst layer was formulated with 20 wt % PVDF for these control experiments. The loading of the catalyst applied to the GDL was chosen so that similar amounts (in mmol) of the total metal would be present on the electrode in the case of InBi and the single-metal catalysts. This was calculated according to the ICP results of metal loading on carbon and In/Bi ratio (see below) and corresponded to 2 mg_{InBi} cm^{-2} for InBi, 1.4 mg_{In} cm^{-2} for In, and 2.8 mg_{Bi} cm^{-2} for Bi. The results are summarized in Figure 1. The InBi catalyst is the best-performing one with a CE of 96%, followed by 93% for In and 74% for Bi.

Catalyst Characterization. The physicochemical characteristics of the catalyst were investigated by means of several techniques.

Scanning Electron Microscopy. The morphology and distribution of the particles on the carbon support were

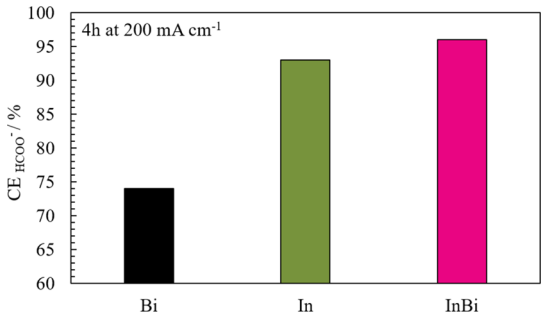

Figure 1. Comparison of current efficiencies of the single-metal catalysts compared to the bimetallic InBi catalyst during 4 h of operation at 200 mA cm^{-2}.

https://doi.org/10.1021/acsaem.1c03156
ACS Appl. Energy Mater. 2022, 5, 1720−1730

investigated by SEM. Some representative pictures are shown in the Supporting Information (Figures S11 and S12), where a comparison of the single-metal catalysts and the InBi catalyst at a similar loading on carbon as well as a comparison of InBi catalysts at different loadings on carbon is shown. In the images, it is possible to see that with the exception of InBi 30 wt % on carbon, the synthesis yields big particles, in the range of hundreds of nanometers, embedded (rather than supported) in the carbon support due to the big size.

Inductively Coupled Plasma Spectroscopy. The elemental composition and loading on carbon were investigated by ICP spectroscopy. The results are shown in the Supporting Information (Figure S13). While the amount of Bi on the carbon support is consistent with the expected one, that of In is lower in both the monometallic and bimetallic samples. During the washing cycles, a brown suspension was observed in the filtrate for the In and InBi catalysts, indicating that some of the metals was leached out. The actual loadings on carbon are 33% for In (53.7% expected), 63.6% for Bi (67.9% expected), and 55.4% for InBi (60% expected) with a weight ratio of In/Bi of 0.6 (expected ratio is 1). This gives a molar composition of approximately 50:50 In/Bi in the bimetallic catalyst (expected, 65:35 In/Bi).

Differential Scanning Calorimetry. Figure 2 shows the results of our differential scanning calorimetry (DSC) analysis of the three catalysts. With DSC, we are able to evaluate the bulk composition as well as the eventual presence of amorphous phases in our materials, making it a useful complement to such techniques as XPS and XRD. During the first cycle (Figure 2a), In and Bi show the characteristic melting points of the metallic phases (156 °C for In and 271 °C for Bi), while the only significant peak in the InBi sample is the one attributable to metallic Bi. InBi only shows minor peaks related to bimetallic phases at 66, 84, and 107 °C, which can, respectively, be attributed to the eutectic phase, the compound $BiIn_2$, and the compound BiIn.[23] The melting points are slightly shifted to lower temperatures compared to the expected ones of 72, 88, and 109 °C. This is possibly due to the existence of these compounds in very small crystalline domains, where the melting point depression effect starts to be significant.[24] A very small peak related to metallic indium (156 °C) is also visible.

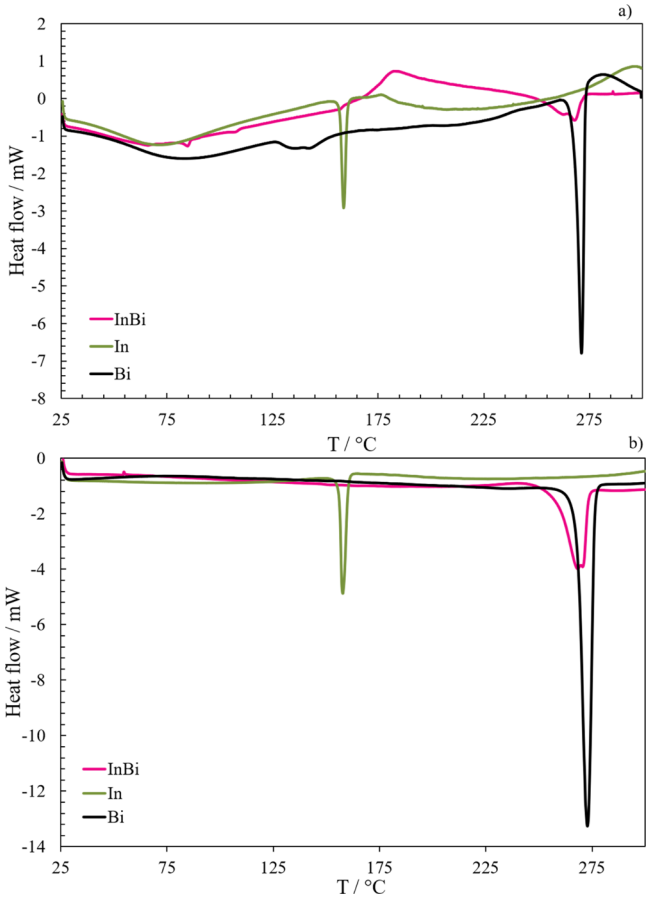

Figure 2. DSC of pure In, pure Bi, and InBi particles supported on carbon: (a) first cycle and (b) second cycle.

During the second cycle (Figure 2b), the DSC spectra are more flat and easily quantifiable, but in the case of the InBi sample, all peaks related to InBi intermetallics and In have disappeared, indicating that exposure to high temperatures can decompose the residual weak In−Bi bonds. The melting point of Bi is shifted to lower temperatures in the InBi catalyst compared to the pure Bi catalyst, and as In is not soluble in the Bi matrix, this is probably due to the existence of metallic Bi in small crystalline domains, rather than to the formation of solid solutions.

X-Ray Photoelectron Spectroscopy. The results of the XPS analysis (Figure S14) indicate that the species In^{3+} make up 98−99% of the observed In in the first layers of our In and InBi particles. The XPS atomic ratios in InBi particles are 80.5% In and 19.5% Bi, indicating that the first few nanometers of the particles are indium-enriched. The In peaks in the InBi particles are shifted positively of 0.2 eV compared to those in the pure In particles, possibly due to the electron-withdrawing effect of the more electronegative Bi atoms, which in turn would increase the oxidizability of In.

X-Ray Diffraction. The X-ray diffraction (XRD) patterns of the three materials are shown in Figure S15. Only reflections relative to the elements in their metallic state can be seen in the diffraction patterns. A small reflection for metallic In is seen in the InBi particles, while all the other peaks can be assigned to metallic Bi, with no reflections assignable to the intermetallic phases.

Electrochemical Measurements. A three-electrode setup was used to characterize our catalysts by CV. The three catalysts were cycled several times in N_2- and CO_2-saturated 0.5 M $KHCO_3$ at 50 mV/s. Figure 3 shows the voltammograms. The comparison of the voltammograms of the three catalysts in the N_2- and CO_2-saturated electrolytes is instead shown in the Supporting Information (Figure S16a,b).

Design of Experiments. The DOE results are shown in Table 3.

Interactive multiple linear regression models generated from the method described in the Experimental Methods section are provided as supporting content as HTML files. Summaries of fit (including the R^2 values and root-mean-square error) and the coefficient estimates and p values for the model terms are listed in the order of statistical significance under the Sorted Parameter Estimates in the Supporting Information (Figures S8 and S10). The null hypothesis of the t test performed for each estimate is that the parameter's coefficient is zero. Therefore, when the p value is low, the null hypothesis is rejected, and the model term is shown to have statistical significance. Furthermore, the lower the p value, the higher is the probability that the parameter is statistically significant.

https://doi.org/10.1021/acsaem.1c03156
ACS Appl. Energy Mater. 2022, 5, 1720−1730

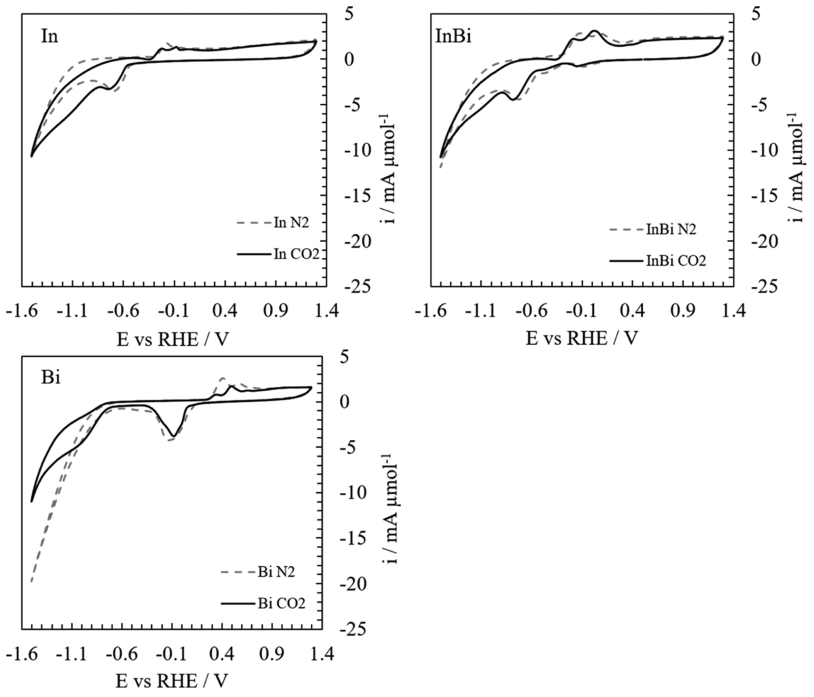

Figure 3. Cyclic voltammograms of In, Bi, and InBi in CO_2-saturated 0.5 M $KHCO_3$ (solid black lines) and N_2-saturated 0.5 M $KHCO_3$ (dashed gray lines).

Table 3. Experimental Design Matrix and Run Results

run number	GDL method number	loading (mg/cm^2)	catalyst on carbon (wt %)	current density (mA/cm^2)	binder in catalyst layer (wt %)	binder type	cell potential	formate current efficiency (%)
1	1	2	30	400	30	PVDF	10.18	68.5
2	1	0.5	30	400	10	PVDF	10.00	93.5
3	1	1.25	90	300	10	PVDF	8.45	69.9
4	2	2	30	400	30	Nafion	9.92	84.1
5	1	2	60	400	20	PVDF	10.09	94.6
6	1	0.5	30	400	20	Nafion	9.43	83.5
7	2	2	90	300	20	Nafion	8.25	93.4
8	1	2	90	400	10	Nafion	9.65	94.2
9	1	2	60	200	30	Nafion	6.84	82.4
10	2	2	90	400	30	PVDF	8.35	28.2
11	1	0.5	90	400	30	PVDF	11.46	23.4
12	2	0.5	90	200	30	PVDF	6.40	86.3
13	1	2	30	300	10	Nafion	8.43	84.6
14	2	1.25	60	400	10	Nafion	8.29	77.2
15	2	0.5	90	400	10	PVDF	9.25	60.0
16	2	0.5	30	400	30	PVDF	9.12	93.1
17	2	0.5	30	200	10	PVDF	6.74	90.3
18	2	0.5	30	300	10	Nafion	8.90	87.4
19	2	0.5	30	200	30	Nafion	6.90	79.7
20	1	0.5	60	300	30	Nafion	9.14	40.2
21	2	2	90	200	10	PVDF	6.77	88.5
22	1	2	90	200	30	PVDF	6.70	23.3
23	2	2	30	200	30	PVDF	6.27	85.4
24	1	0.5	90	200	10	Nafion	7.14	95.4
25	1	1.25	30	200	20	Nafion	6.78	94.1
26	2	1.25	90	200	30	Nafion	6.84	70.3
27	2	2	60	200	10	Nafion	7.00	95.2
28	1	0.5	30	200	30	PVDF	6.11	86.1
29	1	2	30	200	10	PVDF	6.26	77.1
30	2	0.5	90	400	20	Nafion	8.12	99.4
31	2	2	30	400	10	PVDF	9.39	63.4
32	1	1.25	90	400	30	Nafion	10.23	13.4

https://doi.org/10.1021/acsaem.1c03156
ACS Appl. Energy Mater. 2022, 5, 1720−1730

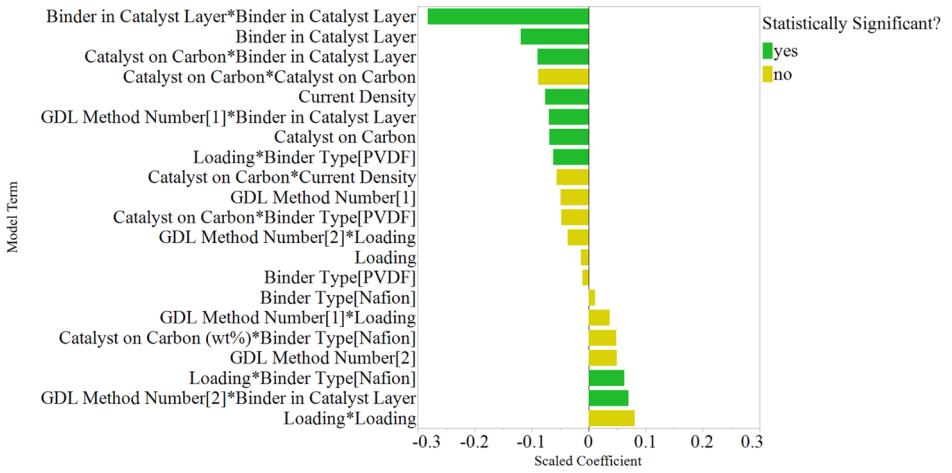

Figure 4. Model term coefficients for scaled factors for the CE toward formate. Terms with p values less than 0.01 are shown as statistically significant.

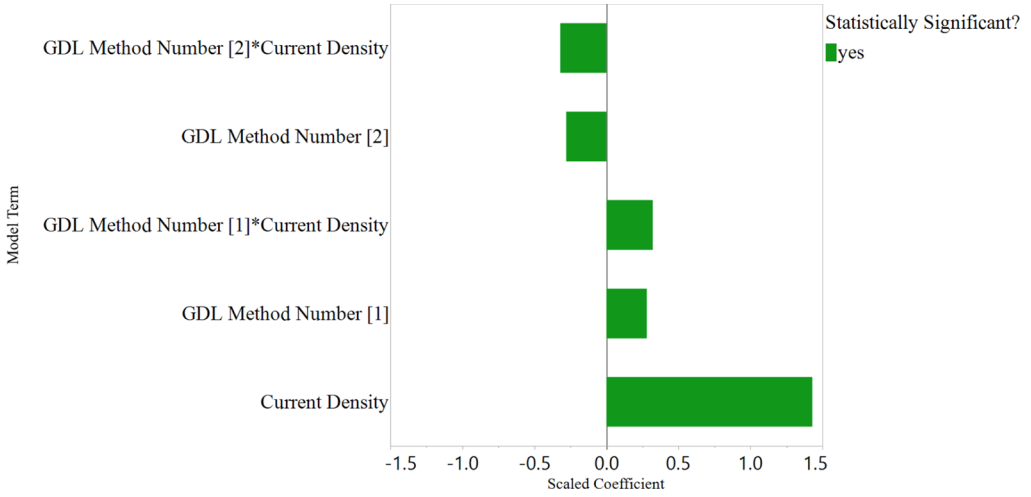

Figure 5. Model term coefficients for scaled factors for the cell potential. Terms with p values less than 0.01 are shown as statistically significant.

Additionally, the three model profilers used for visualizing the respective equations are also shown in the Supporting Information (Figures S17 and S18). The model profilers are only a snapshot of the whole model. The trend for each factor term in the model can be seen in these figures; however, these curves can change if there is a two-factor interaction in the model or can be shifted as other factors are changed.

The coefficients of the model terms indicate the average change in response for every unit increase in the factor term. Comparing these coefficients directly can lead to wrong conclusions as these coefficients are directly affected by the scale of the factor (i.e., current density measured in kA/m^2 mA/cm^2 results in 2 orders of magnitude difference in the numerical value, and thus the coefficient for the single factor model term can vary by two orders of magnitude depending on which unit is used.) Therefore, scaling the factors such that the mean is zero and the range is 2 and then fitting a model with these scaled factors result in coefficients that can be impartially compared and allow for the determination of factors which influence the response the most.[25] The model term coefficients for scaled factors for the CE toward formate and cell potential are shown in Figures 4 and 5.

Extended Operation Experiments. Electrodes used from run number 5 (Table 3) were used for the extended operation experiments because of their high CE toward formate and low amount of salt accumulated in the structure. Each electrode used was run in the DOE for 6 h before operating in the extended run experiments. Separate electrodes were operated at different current densities for these extended experiments. A plot of the CE versus time for the two electrodes is shown in Figure 6.

DISCUSSION

Catalyst Physicochemical Characterization. The enhanced performance of the InBi catalyst, as shown in Figure 1, is in good agreement with the patented results[16] which show that InBi is slightly more selective than an anodized In electrode (80% vs 76% CE) and significantly more selective than nonanodized In (64% CE). In our case, In performs only slightly worse than the InBi catalyst. This may be caused by the fact that the particulate nature of the catalyst enhances the surface exposed, increasing the amount of oxide. The importance of metastable (hydr)oxides for the selectivity of In catalysts for CO_2 reduction to formate has been argued in previous studies.[26,27] The overall enhancement of selectivity is probably attributable to the more favorable mass transport properties of the GDE configuration.

https://doi.org/10.1021/acsaem.1c03156
ACS Appl. Energy Mater. 2022, 5, 1720−1730

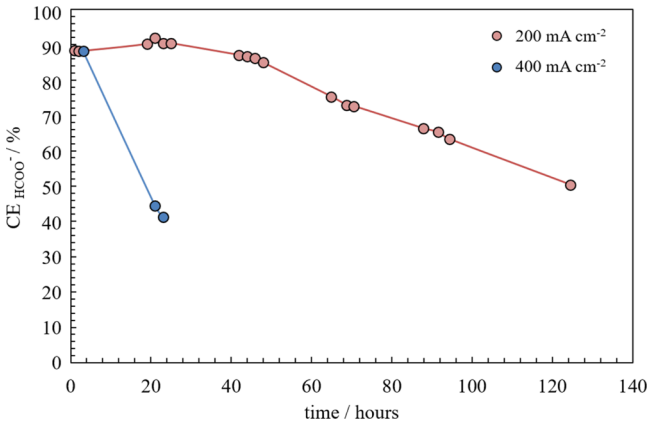

Figure 6. CE toward formate vs time for two electrodes operated for extended hours. The electrodes used for these runs correspond to run number 5 in the DOE. In particular, the catalyst layer consisted of 60 wt % InBi/C with 20 wt % PVDF as a binder and a metal loading on the electrode of 2 mg cm^{-2}.

To understand the reasons behind this increase in selectivity, we characterized the catalyst by means of several techniques. In Figure 2, we show our DSC analysis of the three catalysts. It is noticeable that, while in the single-metal catalysts the melting of pure metals is evident (peak at 156 °C for In and at 271 °C for Bi), in the InBi catalyst, only minor amounts of intermetallic compounds and metallic In are visible, and only the melting of metallic Bi is present, despite the ICP analysis showing an atomic In/Bi ratio of 50:50. The oxides of In and Bi are not visible in the investigated temperature range as their melting points are higher than 300 °C, so it is likely that the missing In peaks in the InBi particles are caused by a high fraction of this metal being in the oxidized state. By integrating the peak areas in Figure 2 and knowing the heats of fusion (3.27 kJ mol^{-1} for In and 11.3 kJ mol^{-1} for Bi) and the total amounts of metal in the samples, we can estimate the amount of metal present in the metallic state, assuming that the remaining part will be in an oxidized state. The intermetallic compounds, not knowing the exact heats of fusion, are impossible to quantify, but the total amount of energy exchanged during their fusion is very small, indicating that only a minor amount of these compounds is present. During the first cycle, in the InBi sample, only 4% of In is present in the metallic state. During the second cycle, the amount of metallic Bi is 60.9% in the pure Bi particles and 56.9% in the InBi particles. The amount of metallic In is 54.5% in the pure In particles and 0% in the InBi particles, indicating that all In present is in the oxide form. Therefore, it seems that the presence of Bi can enhance the oxidizability of In rather than forming intermetallic compounds in our particles, at least after air exposure. This can be explained by the different electronegativities of In and Bi (1.78 vs 2.02). As Bi is a more noble metal, it could favor the oxidation of In in a galvanic corrosion process.

Our XPS analysis (Figure S14) shows that the surface of both In and InBi particles is predominantly oxidized and that the first layers in the InBi particles are enriched in In, with an atomic In/Bi ratio of 80.5:19.5, compared to 50:50 indicated by the ICP analysis. The behavior of the Bi XPS spectrum is somewhat more complex. The Bi peaks in the InBi catalyst are broadened and shifted to a higher binding energy compared to the pure Bi catalyst, which would be counterintuitive if we expect the Bi atoms to simply bear the partial negative charge drawn from In. Such an effect could be caused, for example, by the dispersion of Bi in the In oxide matrix in the form of single atoms or small clusters, which would add layers of complexity to the overall photoemission behavior, compared to the bulk Bi to which it is compared. Similar shifts in XPS spectra with decreasing particle size have been observed earlier.[27] As the Bi results may be difficult to deconvolute and interpret correctly, its XPS spectra were used only for the calculation of the atomic ratios.

In our CV analysis (Figure 3), it is easily noticeable that qualitatively speaking, the cyclic voltammogram of the InBi catalyst is very similar to the one of In. The redox features of Bi, especially the reduction peak around −0.1 V versus RHE, which is a prominent feature in the voltammetry of pure Bi, are barely noticeable. While XPS shows that 80.5% of the metal atoms in the first few nanometers are indium atoms, with the CV, we can see that the electroactive surface is likely even more enriched with In. Therefore, during CO_2 reduction, the catalytic surface is probably composed of a large amount of In, with a small number of Bi inclusions. Note that the current densities reported in the voltammograms are normalized by the amount of μmols on the surface of the electrode. As the currents registered for the redox peaks of In on In and InBi particles are similar, the particle size distribution of the two catalysts should be in a similar range, with the InBi particles possibly having a slightly larger surface area. This is clearer when comparing the In reduction peak around −0.7 V versus RHE in Figure S16 (for the In and InBi catalysts).

Aside from the features related to the metallic surface of the electrode, it is interesting to compare the behavior of the catalysts in the cathodic branch where hydrogen evolution and CO_2 reduction are expected to occur. The overlayed cyclic voltammograms of the three catalysts in the N_2- and CO_2-saturated electrolytes are shown in the Supporting Information (Figure S16a,b). It is clear that the behavior of the InBi catalyst in this cathodic region is very similar to the one of pure In, suggesting that In itself is the main contributor to the CO_2 reduction (or hydrogen evolution) behavior, while Bi seems to slightly enhance its performance in the case of CO_2 reduction.

While it is possible that during the synthesis of the particles some intermetallic compounds may be formed in accordance with the phase diagram of the In−Bi system,[23] it appears that exposure to the atmosphere will cause the In fraction of the particles to segregate on the surface. This is due to the extremely weak bonds formed between In and Bi, as shown by the only slightly exothermic enthalpies of formation of their intermetallic compounds[28] and by the larger tendency of In to be oxidized (ΔH_f^0 Bi_2O_3 = −573.9 kJ mol^{-1} vs ΔH_f^0 In_2O_3 = −925.8 kJ mol^{-1}). Also, the percentage of In in its oxidized state is significantly higher in the InBi particles compared to the pure In particles, not only on the surface but also in the bulk, as shown by DSC. Interestingly, these oxides appear to be entirely amorphous, as they do not show in our XRD analysis (Figure S15). The CV analysis of InBi shows predominantly features related to In, both in the metal redox peaks and in the cathodic branch, confirming that the electrochemically active surface area is predominantly composed of this element. At this stage, we cannot entirely exclude the fact that the difference in selectivity between In and InBi can be caused by small differences in surface area. However, with the evidence presented above, and knowing that a similarly enhanced selectivity is observed also in the electrodes presented in the

https://doi.org/10.1021/acsaem.1c03156
ACS Appl. Energy Mater. 2022, 5, 1720−1730

patent,[16] we would like to propose that the main active phase of our bimetallic catalyst is In, and the effect of the presence of Bi is similar to an anodization process, which has been shown in the literature to improve the selectivity of In catalysts.[27] Moreover, it is possible that the electron-withdrawing effect of Bi on In could partially increase the stability of metastable In oxides, enhancing their presence on the surface and thereby slightly increasing the selectivity of this catalyst compared to a pure In one.

Factors Influencing the Current Efficiency toward Formate. The model for the formate CE has an R^2 value of 0.901, indicating that 90.1% of the variation in the data is explained by this model. The best electrode at 400 mA/cm^2 is predicted to be with the GDL method 2, 30 wt % catalyst on carbon, a loading of 0.5 mg/cm^2, and 20 wt % PVDF. The significant factors and interactions in the model are explained in the next subsections.

Binder Amount, Catalyst on Carbon, and the GDL Production Method. The amount of binder in the catalyst layer has the greatest influence on the CE toward formate. The square term for the binder wt % indicates an optimal amount of binder to be used in the catalyst layer. Additionally, this optimum changes with the varying amounts of catalyst supported on carbon and the GDL type, as indicated by the significance of the interactions between these variables. Table 4 shows the predicted optimal binder for the range of catalysts on carbon and GDLs tested.

Table 4. Predicted Optimal Weight Percentage of Binder in the Catalyst Layer for Different Amounts of Catalyst and GDL Production Methods

		GDL	
		1	2
catalyst on carbon	90%	15.5	18
	30%	18.5	21

During the experiments, the catalyst was observed in the catholyte of the first sample for GDEs that contained only 10 wt % binder, indicating that the catalyst was detaching from the surface. This low level of binder is therefore not enough to hold all of the catalyst onto the GDL. Conversely, when there is too much binder, the active catalytic area can be covered, and the pores that are responsible for transporting CO_2 can become blocked and essentially rendered useless. This is supported by comparing the predicted optima in binder percentage. A lower optimum is predicted for higher amounts of catalyst on carbon. This is because a catalyst layer with 90% support on carbon should be thinner than the one that is 30% supported on carbon for the same loading, and therefore there is less material to bind to the GDL. Additionally, using the same amount of binder in a thinner catalyst layer can result in the catalyst becoming covered more easily, resulting in a decrease in the active catalytic surface area and a lower performance of the electrode.

A lower optimum is also predicted for GDL 1 than for GDL 2. These two GDLs have different characteristics; so, it is not clear which one, or combination, of GDL properties is influencing the performance of the GDE. This result shows that the choice of GDL is important for this reaction, and it is difficult to compare studies when different GDLs are used. Therefore, it is crucial to consider the GDL and how it interacts with the catalyst layer (mainly the amount of binder) when designing future studies.

It is surprising that the interaction between the binder type and binder amount does not show statistical significance. This interaction would indicate that the optimum binder concentration is also dependent on the binder type used. The lack of statistical significance for this interaction suggests that the binder's role in the catalyst layer is primarily to bind the catalyst rather than provide ion conductivity. However, the fact that this interaction does not show significance in this study does not exclude the fact that it could be relevant for other binders. These results only show that there is no significant difference in the optimal binder amounts for Nafion and PVDF. Therefore, this interaction should still be considered with the use of a different binder.

Current Density. As expected, the model shows a negative trend (designated by the negative coefficient) between the current density and the CE toward formate. As the current density increases, the rate of CO_2 conversion also increases, which eventually cannot be sustained due to mass-transfer limitations. This ultimately results in a decrease in the CE toward formate. This mass-transfer limitation can occur at one of several steps, as discussed by Motoo et al.[29] The limit can occur from the supply of the reactant gas to the gas chamber side of GDL, the diffusion of the reactant gas through the GDL to the three-phase boundary, and from the diffusion of the dissolved gas at the three-phase boundary to the catalyst. Although the significance is not as high, the fact that the interaction between the catalyst on carbon and current density shows significance at $\alpha = 0.025$ (Figure S8) suggests that the limitation may be from a lack of accessible catalytic surface area. This interaction indicates that the lower percentage of catalyst supported on carbon performed better at the higher current densities tested (Figure S17). This can be a result of a less dispersed catalyst on carbon and the catalyst layer. The SEM pictures of the three catalysts tested are shown in the Supporting Information (Figure S12). It seems that decreasing amounts of carbon cause an increase in the size of the particles obtained (i.e., the 90% catalyst supported on carbon contains much larger particles than either 60% or 30% catalyst supported on carbon). Additionally, the higher the amount of catalyst on carbon, the thinner the catalyst layer will be, and consequently, fewer layers will be sprayed onto the GDL in the spraying application process. This causes a less evenly dispersed catalyst across the geometrical area and can hinder mass transfer to the catalytic sites.

Loading of Catalyst and Binder Type. The interaction between the catalyst loading and binder type is the last model term that shows significance for $\alpha = 0.01$. This interaction indicates that lower loadings of the catalyst perform better with PVDF as a binder, while higher loadings perform better with Nafion as a binder. There are several characteristics of the binder that could be contributing to this observation, such as the binder density and hydrophobicity. Additionally, Nafion has ion-conducting groups, which could be beneficial at higher loadings when there is a more catalytic surface area. The significance of this effect shows that the binder type used in the catalyst layer should not be overlooked when designing or comparing the experiments for this reaction.

Factors Influencing the Cell Potential. The cell potentials we observed may appear high because of the cell design that was used, nonoptimized electrolyte feed concentrations, low product concentrations, and choice of the

https://doi.org/10.1021/acsaem.1c03156
ACS Appl. Energy Mater. 2022, 5, 1720−1730

membrane. The model for the cell potential has an R^2 value of 0.881, indicating that 88.1% of the variation in the data is explained by this model with only two factors. These factors and interactions are discussed in the following subsections.

Current Density and GDL Production Method. It is no surprise that the current density affects the cell potential the most out of all the factors. This is a consequence of the Butler−Volmer kinetics of the cathodic and anodic reactions as well as the ohmic drop across the cell. The interaction between the GDL method and current density has the second largest effect on the cell potential. This interaction should be expected due to the different conductivities of the GDLs; however, the trend observed for the effect of the GDL on the cell potential is the opposite of what would be expected based solely on these characteristics. Table 5 shows the surface conductivity, conductance through, and porosity of the GDLs produced from methods 1 and 2.

Table 5. GDL Characteristics

GDL	surface conductivity (S/m)	conductance through GDL (S)	porosity by Hg intrusion (%)	water contact angle (°)
1	591	249	69	137
2	365	59	53	141

The results from these experiments show that GDL 1 has a lower conductivity as the slope of the cell potential versus current density curve is seen to be larger in Figure S18 for GDL 1. It is possible that the conductivity of the electrode changes depending on how wet it becomes during operation due to the differences in the electrode's porosity, hydrophobicity, or stability. Wetting of the electrode could occur more in GDL 1 because of its much higher porosity and lower hydrophobicity than GDL 2, as seen in Table 5. Additionally, some electrodes were observed to have a lot of salt accumulation on the back and in the pores of the GDL. In order for this salt accumulation to happen, some of the electrolyte had to penetrate the GDL during operation, which would directly affect the conductivity of the electrode and thus the cell potential.

Extended Stability Experiments. The electrode operated at 200 mA/cm^2 achieved 130.5 h of total operation (including the hours of operation from the DOE experiment) above 50% CE toward formate. Additionally, this electrode operated above 85% CE toward formate for nearly 54 h. On the other hand, the electrode that was run at 400 mA/cm^2 dropped drastically in the CE toward formate in less than 27 h of total operation. This shows that the current density can extremely affect the lifetime of these electrodes. We suggest that the progressive deactivation of the catalyst can be due to a combination of factors. First, the fact that the activity can somewhat be extended by circulating clean water and exposing the electrode to air (as discussed in the Experimental Methods section) suggests that accumulation of salt on the catalyst to bind active sites and the progressive loss of the metastable (hydr)oxides (the most active phase for CO_2 reduction) may play a role. Second, the highly alkaline environment reached during operation at high current density can contribute to the chemical degradation of the binder, decreasing its mechanical stability. Another DOE with the goal of determining which catalyst layer and GDL factors affect this electrode lifetime the most could lead to major insights into the cause of deactivation of these electrodes and/or the best formulation for long lifetime electrodes.

CONCLUSIONS

In conclusion, we have shown that InBi catalysts prepared with our method are slightly more selective than In catalysts and markedly more selective than Bi catalysts prepared with the same method. This effect seems to be due to the fact that Bi, in a process that may be similar to galvanic corrosion, increases the fraction of In in its oxidized state, a process that induces the segregation of this metal to the surface of the particles. The particles with a surface enriched in indium oxides, in turn, would increase the selectivity as this phase has been shown to be the most active for CO_2 reduction to formate.

Moreover, we took a holistic approach in optimizing a GDE for this reaction by using a DOE to identify the crucial factors and interactions of a GDE that affect the CE toward formate and cell potential. Nearly one-third of the GDEs produced for these experiments achieved over 90% CE toward formate at current densities ≥200 mA/cm^2. The binder amount in the catalyst layer affects the CE toward formate the most with the InBi catalyst. There appears to be an optimal binder amount that is dependent on the amount of catalyst supported on carbon and the GDL used. Although this optimal binder amount does not appear to depend on the binder type, only two binders were tested, so this interaction should not be overlooked when testing different binders in the future. The 30 wt % catalyst supported on carbon was shown to perform better at higher current densities due to better dispersion on the carbon support and more uniform distribution across the geometrical area of the electrode, which enhances the mass transfer of CO_2 to the catalyst surface. Additionally, Nafion shows to be better than PVDF when higher loadings are used.

The current density and GDL are shown to affect the cell potential the most as these two factors are able to explain over 88% of the variation in the data. The cell potentials reported in this study are high because electrolyte feeds, product concentrations, membrane used, and cell design were not optimized. These factors, along with the GDL, should be studied in a holistic approach to better optimize the cell potential.

Finally, the stability of the electrode was assessed by operating two of the same electrodes at different current densities until the CE toward formate decreased below 50%. The loss of activity of the electrode could cause electrode instability and lead to salt accumulation inside the structure, or the salt could inherently be accumulated in these electrodes, which could cause a decrease in the performance of the electrode.

The two electrodes operated for extended hours were the DOE experiment number 5 electrodes. One electrode operated at 200 mA/cm^2 above 50% CE for an additional 124.5 h. However, the other electrode ran for less than 24 additional hours at 400 mA/cm^2 before the CE toward formate decreased to below 50%. This shows that the operating current density considerably affects the lifetime of the electrodes. A future study could look at several of the factors affecting the stability outlined in this study and their effect on the lifetime of the electrodes to potentially find ways to operate for longer lifetimes at current densities greater than 200 mA/cm^2.

https://doi.org/10.1021/acsaem.1c03156
ACS Appl. Energy Mater. 2022, 5, 1720−1730

■ ASSOCIATED CONTENT

Supporting Information

The Supporting Information is available free of charge at https://pubs.acs.org/doi/10.1021/acsaem.1c03156.

Interactive profilers showing the models derived from the DOEs for CE and cell potential (ZIP)

Prepared GDL; repeat experiments; comparison of models considered for the two responses; full model equations for the two selected models; and SEM, ICP, XPS, XRD, and CV results of the prepared catalysts (PDF)

■ AUTHOR INFORMATION

Corresponding Author

Klaas Jan P. Schouten − *Avantium Chemicals BV, 1014 BV Amsterdam, The Netherlands;* Present Address: Teijin Aramid BV, Tivolilaan 50, 6824 BW Arnhem, The Netherlands; orcid.org/0000-0003-4792-0085; Email: KlaasJan.Schouten@teijinaramid.com

Authors

Matthew F. Philips − *Avantium Chemicals BV, 1014 BV Amsterdam, The Netherlands; Leiden Institute of Chemistry, Leiden University, 2300 RA Leiden, The Netherlands;* orcid.org/0000-0003-2767-2117

Davide Pavesi − *Avantium Chemicals BV, 1014 BV Amsterdam, The Netherlands; Leiden Institute of Chemistry, Leiden University, 2300 RA Leiden, The Netherlands;* orcid.org/0000-0002-3204-4580

Tim Wissink − *Inorganic Materials and Catalysis, Eindhoven University of Technology, 5600 MB Eindhoven, The Netherlands*

Marta C. Figueiredo − *Inorganic Materials and Catalysis, Eindhoven University of Technology, 5600 MB Eindhoven, The Netherlands*

Gert-Jan M. Gruter − *Avantium Chemicals BV, 1014 BV Amsterdam, The Netherlands; Van't Hoff Institute for Molecular Sciences, University of Amsterdam, 1090 GD Amsterdam, The Netherlands*

Marc T. M. Koper − *Leiden Institute of Chemistry, Leiden University, 2300 RA Leiden, The Netherlands*

Complete contact information is available at: https://pubs.acs.org/10.1021/acsaem.1c03156

Author Contributions

#M.F.P. and D.P. contributed equally to this work.

Notes

The authors declare no competing financial interest.

■ ACKNOWLEDGMENTS

This work was supported by the European Commission under contract 722614 (Innovative training network ELCoREL).

■ REFERENCES

(1) Seh, Z. W.; Kibsgaard, J.; Dickens, C. F.; Chorkendorff, I.; Nørskov, J. K.; Jaramillo, T. F. Combining theory and experiment in electrocatalysis: Insights into materials design. *Science* **2017**, *355*, No. eaad4998.

(2) Lu, X.; Leung, D. Y. C.; Wang, H.; Leung, M. K. H.; Xuan, J. Electrochemical Reduction of Carbon Dioxide to Formic Acid. *ChemElectroChem* **2014**, *1*, 836−849.

(3) Schuler, E.; Ermolich, P. A.; Shiju, N. R.; Gruter, G. J. M. Monomers from CO_2: Superbases as Catalysts for Formate-to-Oxalate Coupling. *ChemSusChem* **2021**, *14*, 1517.

(4) Meisel, T.; Halmos, Z.; Seybold, K.; Pungor, E. The thermal decomposition of alkali metal formates. *J. Therm. Anal.* **1975**, *7*, 73−80.

(5) Boswell, M. C.; Dickson, J. V. The action of sodium hydroxide on carbon monoxide, sodium formate and sodium oxalate. *J. Am. Chem. Soc.* **1918**, *40*, 1779−1786.

(6) Durst, J.; Rudnev, A.; Dutta, A.; Fu, Y.; Herranz, J.; Kaliginedi, V.; Kuzume, A.; Permyakova, A. A.; Paratcha, Y.; Broekmann, P.; Schmidt, T. J. Electrochemical CO_2 Reduction − A Critical View on Fundamentals, Materials and Applications. *Chimia* **2015**, *69*, 769−776.

(7) Oloman, C.; Li, H. Electrochemical Processing of Carbon Dioxide. *ChemSusChem* **2008**, *1*, 385−391.

(8) Martín, A. J.; Larrazábal, G. O.; Pérez-Ramírez, J. Towards sustainable fuels and chemicals through the electrochemical reduction of CO_2 : lessons from water electrolysis. *Green Chem.* **2015**, *17*, 5114−5130.

(9) Verma, S.; Kim, B.; Jhong, H.-R. M.; Ma, S.; Kenis, P. J. A. A Gross-Margin Model for Defining Technoeconomic Benchmarks in the Electroreduction of CO_2. *ChemSusChem* **2016**, *9*, 1972−1979.

(10) Hori, Y. Electrochemical CO_2 Reduction on Metal Electrodes. *Modern Aspects of Electrochemistry*; Springer Science & Business Media, 2008; pp 89−189.

(11) Higgins, D.; Hahn, C.; Xiang, C.; Jaramillo, T. F.; Weber, A. Z. Gas-Diffusion Electrodes for Carbon Dioxide Reduction: A New Paradigm. *ACS Energy Lett.* **2019**, *4*, 317−324.

(12) Philips, M. F.; Gruter, G.-J. M.; Koper, M. T. M.; Schouten, K. J. P. Optimizing the Electrochemical Reduction of CO2 to Formate: A State-of-the-Art Analysis. *ACS Sustain. Chem. Eng.* **2020**, *8*, 15430.

(13) Kopljar, D.; Inan, A.; Vindayer, P.; Wagner, N.; Klemm, E. Electrochemical reduction of CO_2 to formate at high current density using gas diffusion electrodes. *J. Appl. Electrochem.* **2014**, *44*, 1107−1116.

(14) Löwe, A.; Schmidt, M.; Bienen, F.; Kopljar, D.; Wagner, N.; Klemm, E. Optimizing Reaction Conditions and Gas Diffusion Electrodes Applied in the CO2 Reduction Reaction to Formate to Reach Current Densities up to 1.8 A cm^{-2}. *ACS Sustain. Chem. Eng.* **2021**, *9*, 4213−4223.

(15) Yi, L.; Chen, J.; Shao, P.; Huang, J.; Peng, X.; Li, J.; Wang, G.; Zhang, C.; Wen, Z. Molten-Salt-Assisted Synthesis of Bismuth Nanosheets for Long-term Continuous Electrocatalytic Conversion of CO_2 to Formate. *Angew. Chem., Int. Ed.* **2020**, *59*, 20112−20119.

(16) Parajuli, R.; Ansovini, D.; Philips, M. F.; Schouten, K. J. P. Catalyst system for catalyzed electrochemical reactions and preparation thereof, applications and uses thereof. WO 2019141827 A1.

(17) Thompson, J. *Design and Analysis in Chemical Research*; Tranter, R. L., Ed.; CRC Press, 2000; pp 85−110.

(18) Philips, M. F.; Ansovini, D.; Figueiredo, M. C. C.; Krasovic, J. Method for the Preparation of a Gas Diffusion Layer and a Gas Diffusion Layer Obtained or Obtainable by Such Method. WO 2020165074 A1, 2020.

(19) SAS Institute Inc. *JMP 14 Design of Experiments Guide*, 2018; pp 241−294.

(20) Ansovini, D.; Philips, M. F.; Krasovic, J.; Figueiredo, M. C. C.; Schouten, K. J. Formation of Formic Acid with the Help of Indium-Containing Catalytic Electrode. WO 2021122323 A1, 2021.

(21) Claeskens, G.; Hjort, N. L. *Model Selection and Model Averaging*; Cambridge University Press, 2006.

(22) Klimberg, R.; McCullough, B. D. *Fundamentals of Predictive Analytics with JMP*; SAS Institute Inc, 2013.

(23) Okamoto, H.; Schlesinger, M. E.; Mueller, E. M. Bi (Bismuth) Binary Alloy Phase Diagrams. *J. Alloy Phase Diagrams* **2016**, *3*, 201.

(24) Allen, G. L.; Bayles, R. A.; Gile, W. W.; Jesser, W. A. Small particle melting of pure metals. *Thin Solid Films* **1986**, *144*, 297−308.

(25) SAS Institute Inc. *JMP 14 Fitting Linear Models*, 2018.

(26) Pander, J. E.; Baruch, M. F.; Bocarsly, A. B. Probing the Mechanism of Aqueous CO_2 Reduction on Post-Transition-Metal Electrodes using ATR-IR Spectroelectrochemistry. *ACS Catal.* **2016**, *6*, 7824−7833.
(27) Detweiler, Z. M.; White, J. L.; Bernasek, S. L.; Bocarsly, A. B. Anodized indium metal electrodes for enhanced carbon dioxide reduction in aqueous electrolyte. *Langmuir* **2014**, *30*, 7593−7600.
(28) Kulikova, T.; Mayorova, A.; Shubin, A.; Bykov, V.; Shunyaev, K. Bismuth-indium system: Thermodynamic properties of liquid alloys. *Kovove Mater.* **2016**, *53*, 133−137.
(29) Motoo, S.; Watanabe, M.; Furuya, N. Gas diffusion electrode of high performance. *J. Electroanal. Chem. Interfacial Electrochem.* **1984**, *160*, 351−357.

https://doi.org/10.1021/acsaem.1c03156
ACS Appl. Energy Mater. 2022, 5, 1720−1730